High-pressure phase transitions of $ScPO_4$ and YPO_4

F. X. Zhang, J. W. Wang, M. Lang, J. M. Zhang, and R. C. Ewing*
Department of Geological Sciences, The University of Michigan, Ann Arbor, Michigan 48109, USA

L. A. Boatner
Materials Science and Technology Division and Center for Radiation Detection Materials and Systems, Oak Ridge National Laboratory, Oak Ridge, Tennessee 37831, USA

(Received 14 July 2009; revised manuscript received 29 October 2009; published 24 November 2009)

$ScPO_4$ and YPO_4 with the tetragonal zircon-structure were studied at room temperature and pressures up to ~50 GPa. Pressure-induced phase transitions to the sheelite structure occur at 30 GPa for $ScPO_4$ and 16.3 GPa for YPO_4, respectively. In addition to the scheelite-type high-pressure phase, an intermediate phase with the monoclinic monazite-type structure formed during the phase transition process of YPO_4. The high-pressure phases of $ScPO_4$ and YPO_4 are not quenchable on pressure release. The pressure dependence of the total energy of the different phases was calculated using density-functional method, and the results confirm the experimentally observed phase relations under pressure. Structural parameters and compressibility of each phase were determined by refinement of the x-ray diffraction patterns. The high-pressure phase of $ScPO_4$ has a very large bulk modulus [376(8) GPa].

DOI: 10.1103/PhysRevB.80.184114 PACS number(s): 61.50.Ks, 61.66.Fn, 72.80.Ga

I. INTRODUCTION

ABO_4 ternary oxides are important to a variety of geophysical and geochemical applications, as they are common accessory minerals (i.e., zircon: $ZrSiO_4$; and monazite: $CePO_4$) in a wide variety of rock types in the Earth's upper mantle.[1–4] The structure-type that forms, i.e., tetragonal zircon vs monoclinic monazite, depends, in part, on the size of the *A*-site cation. For the orthophosphates, both the zircon-type and monazite-type structures occur at ambient conditions. The light rare-earth elements (*Z* less than that of Gd) form the monoclinic monazite-type structure, but the heavier rare-earth elements (including Sc and *Y*) form the tetragonal zircon-type structure. The rare-earth elements at the boundary of these structure types, such as Gd, Tb, and Dy, may occur as both structures at ambient conditions as a function of their thermal history. The structural stability and thermodynamic properties of rare-earth orthophosphates have been systematically investigated.[5] In both the monazite- and zircon-type phosphates, phosphorous is in fourfold coordination with oxygen forming isolated tetrahedra. The monazite structure is denser because the coordination of the *A*-site cation (including Sc^{3+} and Y^{3+}) is ninefold. These phosphates have excellent high-temperature properties, high radiation damage tolerance and good chemical stabilities.[6,7] They have been proposed in recent years as host materials for the incorporation and disposal of high-level radioactive nuclear waste.[8–10] In addition, orthophosphates are of great interest because of their optical properties.[11–13]

Phase transitions of the ABO_4 ternary oxides at high-pressure have been widely investigated since the 1960's,[14] and a close relation between cation size and crystal structure was revealed. Fukunaga and Yamaoka[15] have summarized the general trend of the phase transition sequence under pressure as a function of the size of cations. Generally, the radius ratios of r_A/r_O and r_B/r_O between cations and oxygen increase with pressure, resulting in an increase in the cation coordination in the high-pressure phases. A more complete review on various ABO_4 compounds was completed recently.[16] However, there are rare reports on the pressure-induced phase transitions of rare-earth phosphates. Recently, we have reported the pressure-induced phase transition behavior in $YbPO_4$ and $LuPO_4$,[17] which is similar with that of zircon at high-pressures. Stavrou *et al.*[18] have also measured the Raman spectrum of $TbPO_4$ and an irreversible phase transition was reported at pressure of ~9.5 GPa, but the structure of the high-pressure phase remains unknown.

$ScPO_4$ and YPO_4 are isostructural with the heavy rare-earth phosphates, and they both crystallize in the zircon-type structure at ambient conditions. However, their behavior with increasing pressure is different from that of zircon. In this paper, the structural properties of $ScPO_4$ and YPO_4 were studied by synchrotron powder x-ray diffraction (XRD), Raman scattering, and theoretical calculations. In addition to the zircon-type to scheelite-type phase transition at high-pressure in both systems, an intermediate phase with the monazite-type structure was found during the phase transition process of YPO_4. The different structural behaviors of these phosphates are found to be due to the different size of cations.

II. EXPERIMENTAL METHODS

Single crystals of $ScPO_4$ and YPO_4 were grown by a high-temperature flux method. Details of the synthesis process were described elsewhere.[5] In carrying out the XRD measurements, single crystals were crushed into fine powders in a mortar until no obvious separated spots can be found in the diffraction image, and the average grain size was estimated to be less than 2 μm. High-pressure experiments were performed with diamond anvil cell (DAC) techniques and hardened stainless steel gaskets were used for all the high-pressure experiments. Standard methanol/ethanol mixture with or without water was used as the pressure transmitting medium, which maintains good hydrostatic condi-

tions below 10–12 GPa. The *in situ* high-pressure XRD measurements were performed using a synchrotron radiation x-ray source (0.4066 Å) at X17C station of National synchrotron light source (NSLS), Brookhaven National Laboratory, or by using a monochromated x-ray beam (0.4960 Å) at the Cornell high-energy synchrotron source (CHESS). The beam spot size is less than 25×25 μm^2 in NSLS and ~50 μm at CHESS. The diffraction rings were recorded with a charge-coupled device (CCD) detector or a Mar345 image plate detector. All of the XRD patterns were integrated from the images using the FIT2D software package.[19] The pressure in all of the experiments was measured by the standard ruby fluorescence method,[20] and the XRD patterns were refined by Rietveld method (Fullprof in the software package Winplotr)[21] based on the known structural models. In order to obtain the unit cell parameters of the high-pressure phase of $ScPO_4$, an additional XRD experiment was made at 16-ID-D beam of HPCAT, Argonne National Laboratory with monochromated beam of 0.4125 Å and beam size ~5 μm.

Raman measurement was performed at U2 station of NSLS. Small pieces of $ScPO_4$ and YPO_4 were loaded in the same pressure chamber. The activate source is 514.3 nm green light from an Ar laser with power of 300 mW. The backscattering light was collected with a liquid nitrogen cooled CCD detector.

Quantum mechanical calculations were performed using the density-functional theory (DFT) framework, and plane-wave basis sets as implemented in the VASP package.[22] The projector-augmented wave (PAW) method[23] and exchange correlation as parameterized by the Perdew-Wang 91 (PW91) functional[24,25] were applied in the generalized gradient approximation (GGA-PAW).[26] The total energy and volume calculations for the two systems were completed by optimizing the structures without symmetry constraints. The Monkhorst-Pack scheme for integration in the Brillouin zone is adopted. Test runs were performed to test the energy convergence on *k*-point grid and energy cutoff. A $5\times5\times5$ *k*-point grid is used for the monoclinic and tetragonal phases, and a $7\times7\times4$ *k*-point grid is used for high-pressure tetragonal phase. The energy cutoff for the plane-wave basis set is 520.00 eV (38.22 Ry) for all the calculations. These parameters are sufficient for energy convergence.

III. RESULTS AND DISCUSSION

A. XRD measurements

The flux grown crystals of $ScPO_4$ and YPO_4 are transparent and display good crystal forms. The selected powder XRD patterns of $ScPO_4$ and YPO_4 at various pressures are shown in Figs. 1(a) and 1(b), respectively. The intensity of the XRD pattern of $ScPO_4$ is not strong and a small amount of impurities from the residual flux were occasionally observed in the starting material. With the increase in pressure, a new broad peak at two theta around 8.7° appeared clearly in the pattern after 34.2 GPa, which indicates a pressure-induced phase transition. The peak became stronger at higher pressures and more of the sample was transformed to the high-pressure phase(s). However, up to 45 GPa, the zircon-type $ScPO_4$ phase is still observed. The broad peak is the

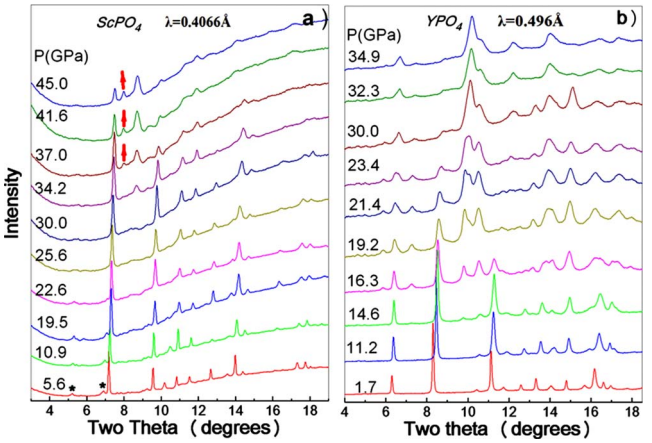

FIG. 1. (Color online) Selected XRD patterns of phosphates at various pressures. (a) $ScPO_4$ measured at NSLS (λ=0.4066 Å). Peaks marked with star symbols are due to the residual impurity from the flux during crystal growth. New peaks are clearly observed in the pattern at 34.2 GPa. The peaks marked with up arrows are due to impurity or other minor phase transitions. (b) YPO_4 measured at CHESS (λ=0.496 Å). The monazite-type high-pressure phase is clearly observable at 16.3 GPa (or even earlier). The pattern after 30 GPa is a combination of monazite- and scheelite-type high-pressure phases.

strongest diffraction maxima of (013) and (112) of the scheelite-type structure. The XRD pattern of $ScPO_4$ at 34.2 GPa was refined as a mixture of the zircon-type and scheelite-type high-pressure phases [Fig. 2(b)]. The XRD patterns of the high-pressure phase of $ScPO_4$ were very weak. In order to increase the XRD intensity for $ScPO_4$, an additional experiment was performed at HPCAT. The pressure-induced phase transitions measured at HPCAT were similar to the patterns shown in Fig. 1(a). The unit cell parameters of the high-pressure phase of $ScPO_4$ were derived by Rietveld refinement of the patterns measured at HPCAT. In addition to the phase transition to the high-pressure scheelite-type phase, another peak appeared in the high-pressure XRD patterns measured at both stations [shown as arrows pointing upwards in Fig. 1(a)] at a lower diffraction angle, which could not be indexed as a diffraction peak of either of the two known phases. This peak may originate from some impurities in the sample or be another minor phase transition of $ScPO_4$ at high pressures.

Because of the larger cation size, YPO_4 has a much lower critical transition pressure. At 14.6 GPa (or even lower pressures), a new phase is clearly evident from the XRD patterns [Fig. 1(b)]. The XRD pattern of the high-pressure phase of YPO_4 is very different from the patterns of the high-pressure phases of $YbPO_4$ and $LuPO_4$ previously observed.[16] Further analysis revealed that they may be attributed to a lower-symmetry monazite-type phase. The zircon-type YPO_4 nearly completely transformed to the monazite-type high-pressure phase at pressure above 19.2 GPa because the second strongest peak (112) at two theta angle of 11.2° disappeared completely in the pattern. The XRD pattern of YPO_4 at 16.3 GPa was refined as a mixture of monazite-type and zircon-type phases [Fig. 2(d)], and the results indicated a 3.2% volume shrinkage during the transition process. With a

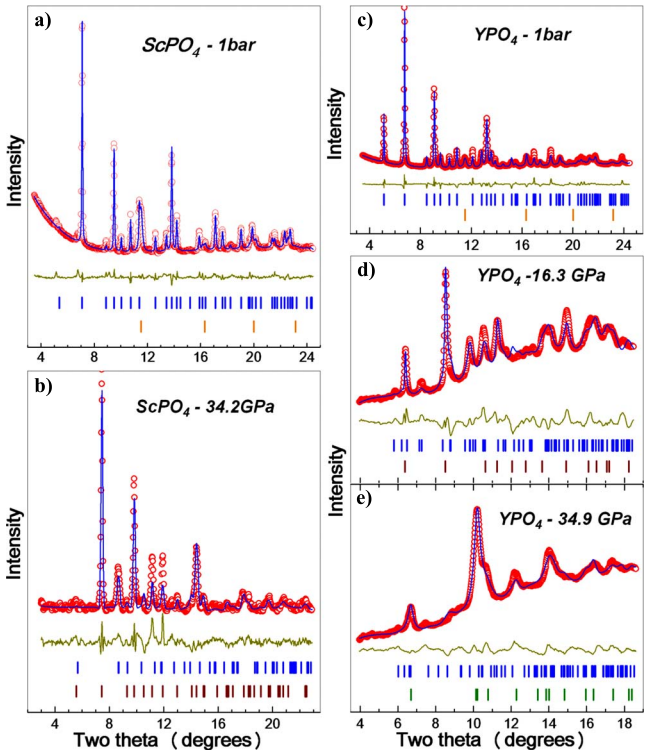

FIG. 2. (Color online) Rietveld refinement results of the observed XRD patterns. (a) $ScPO_4$ at ambient conditions is the zircon-type structure [small amount of Fe (from the steel gasket) and impurities (marked with * symbols)]; (b) XRD pattern of $ScPO_4$ at 34.2 GPa refined with the mixture of zircon-type and monazite-type phases; (c) YPO_4 at room conditions is a pure zircon-type structure; (d) XRD pattern of YPO_4 at 16.3 GPa refined with the mixture of zircon- and monazite-type structures; and (e) XRD pattern of YPO_4 at 34.9 GPa refined with a mixture of monazite- and scheelite-type structures. The patterns on d and e are measured at CHESS with 0.496 Å x-ray beam and other patterns are measured in NSLS with 0.4066 Å x-ray beam.

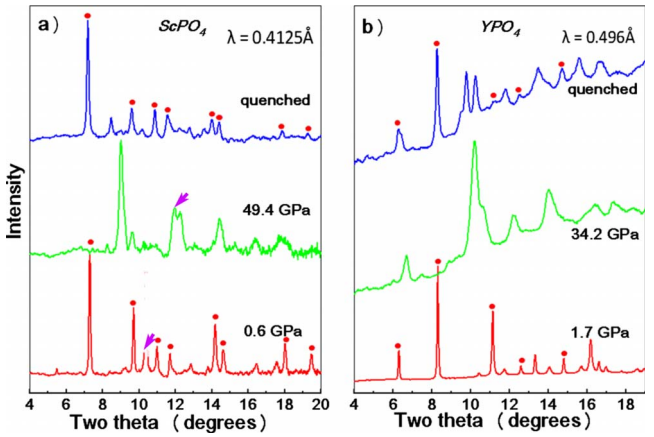

FIG. 3. (Color online) The XRD patterns of during pressure releasing process for (a) $ScPO_4$ and (b) YPO_4. The arrows in Fig. 3(a) show the peaks from pressure medium (water). In the quenched sample, the reflections from the starting zircon-type structure (marked with solid spots) are clearly observed, but the high-pressure phases are still detectable in the experimental time scale (especially to YPO_4).

further increase in pressure, the profile of the XRD pattern changed at pressures above 30 GPa, suggesting that another phase transition has occurred.

The XRD patterns of YPO_4 at pressures higher than 30 GPa are very similar to the patterns of scheelite-type structure, but they contain some extra peaks, such as the triple (or more) peaks at the two theta angle between 5° and 7°. These peaks cannot be attributed to the scheelite-type structure. Analysis of XRD patterns indicated a mixture of two phases for the YPO_4 at pressures greater than 30 GPa. The XRD pattern at 34.9 GPa can be refined as a mixture of monazite-type and scheelite-type phases [Fig. 2(e)]. Thus, the pressure-induced phase transitions of $ScPO_4$ and YPO_4 are different. The zircon-type YPO_4 first transformed to a high-pressure monazite-type phase at 14.6 GPa and then to a scheelite-type phase at higher pressures. The phase transitions from zircon-type $ScPO_4$ and monazite-type YPO_4 to scheelite-type phases are sluggish at room temperature. The sluggish phase-transition behavior at ambient conditions has been previously observed in the studies of zircon[27,28] and other zircon-type ABO_4 compounds,[29] because the phase transition is displacive, but high temperature greatly enhances the transition.[30]

At room temperature, it may be difficult to get a single high-pressure phase for $ScPO_4$ and YPO_4. For $TbPO_4$, we observed a transition sequence similar to that of YPO_4, however, up to 60 GPa, the product is still a mixture of the scheelite- and monazite-type phases. The high-pressure phases of $ScPO_4$ and YPO_4 are not stable at room conditions. Figure 3 shows the XRD patterns of $ScPO_4$ and YPO_4 during the pressure unloading process. The starting zircon-type phase was recovered in the quenched sample, although some strong diffraction maxima from the high-pressure phases are still observable during the time scale of our experiments.

The unit cell parameters of the different phases in $ScPO_4$ and YPO_4 that form as a function of pressure were determined by Rietveld refinement of the XRD patterns. The pressure dependence of the unit cell volume for $ScPO_4$ and YPO_4 are plotted in Figs. 4(a) and 4(b), respectively. The volume decreased about 12.6% at 30 GPa for $ScPO_4$ during the phase transition to the scheelite-type high-pressure phase. For YPO_4, the zircon-type phase transformed to monazite-type high-pressure phase at 16.3 GPa with a volume decrease in 3.2% and further transformed to the scheelite-type high-pressure phase at 32 GPa with 6.8% volume decrease. Fitting the P-V curves with Birch-Murnagham equation of state yields bulk moduli of 203(7) GPa and 186(5) GPa for the zircon-type $ScPO_4$ and YPO_4, respectively. The P-V curve of the corresponding high-pressure phases indicated that they are less compressible. Results obtained by fitting indicated that the monazite-type high-pressure phase of YPO_4 has a bulk modulus of 260(29) GPa, when its pressure derivative at zero pressure is fixed at 4. The scheelite-type high-pressure phase is a dense form and should have larger bulk modulus. The two data points for scheelite-type YPO_4 do not give a reliable value for the bulk modulus. Fitting the volume data for scheelite-type $ScPO_4$ yielded a very large bulk modulus of 376(8) GPa (B_0'=4). This is even greater than

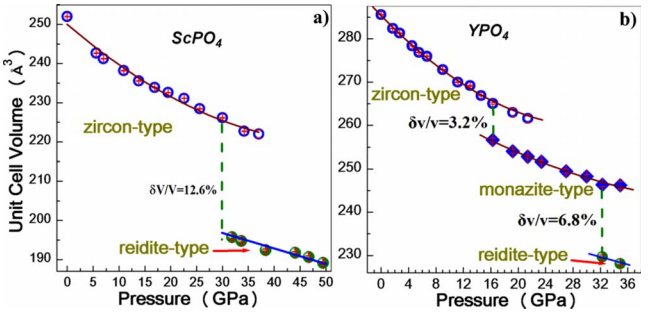

FIG. 4. (Color online) Pressure dependence of the unit cell volume of (a) $ScPO_4$ and (b) YPO_4. There is a volume collapse of ~12.6% at 30–34 GPa for $ScPO_4$ during the phase transition from zircon-type to scheelite-type high-pressure phase. The volume collapse for YPO_4 is 3.2% at 16.3 GPa for the phase transition from zircon-type to monazite-type and 8.2% at 32.3 GPa from the monazite-type to scheelite-type.

that of reidite ($ZrSiO_4$)—the high-pressure form of zircon (301 GPa),[31] and much larger than the values of scheelite-type $YbPO_4$ and $LuPO_4$.[17] The large bulk modulus suggests that the high-pressure form of $ScPO_4$ may be a superhard material. Unfortunately, the scheelite-type high-pressure phase of $ScPO_4$ could not be quenched to room conditions.

The bulk modulus of silicates and some binary oxides was found to be directly correlated to the compressibility of the *A*-cation coordination polyhedra,[32] and it obeys a linear relationship to the compressibility of AO_8 polyhedron in the following empirical formula[33] to most zircon-related ABO_4 structures,

$$B_0 = 610(110)\frac{z_A}{d_{\text{A-O}}^3}, \tag{1}$$

where B_0 is the bulk modulus in GPa, z_A is the formal charge of *A* cations ($1 \leq z_A \leq 4$), and $d_{\text{A-O}}$ is the average *A*-O distance (Å) in the AO_8 polyhedron. To most ABO_4 compounds, BO_4 tetrahedra are interconnected through O-*A*-O bonds, and the *B*-O bonds in BO_4 tetrahedra are shorter and stronger than the *A*-O bond in AO_8 polyhedra. As a result, the compressibility of the whole lattice is mainly related to the compressibility of AO_8 polyhedra. The linear relationship between bulk modulus and the charge density of *A* cation is consistent with the fact that AO_8 polyhedra exhibiting a larger electronic cloud inside the polyhedral than those AO_8 with a lower *A*-cation charge density. The predicted bulk modulus with the above formula fit the observations to most silicates and transition metal oxides.[16,32] However, the predicted bulk modulus of phosphates are obvious lower than the experimental results, especially to the scheelite-type structures.[17] At normal conditions, the bonding distances of Sc-O and Y-O in zircon-type $ScPO_4$ and YPO_4 are 2.2016 and 2.3365 Å, respectively, and the predicted bulk modulus are 171 and 144 GPa, which are less than the observed values (203 GPa for $ScPO_4$ and 186 GPa for YPO_4). In phosphates, cation P^{5+} is four-coordinated and there is an extra electron transfer from the $P^{5+}O_4$ tetrahedron to the neighbor AO_8 polyhedra, and as a result, the effected electron density in AO_8 polyhedra increased. If the effective charge of *A* cation is taken as 3.6, the calculated bulk modulus is 205 GPa for the zircon-type $ScPO_4$ and 169 GPa for YPO_4, which fit the experimental results quite well. The scheelite-type structure is a dense form of the zircon-type structure, and the AO_8 polyhedra are compressed. For example, the bond distance of Zr-O in reidite (scheelite-type zircon, $ZrSiO_4$) is 2.22 Å, which is smaller than that in zircon (2.268 the bond distance of Zr-O), while the Si-O bond distance in reidite is 1.68 Å and larger than that in zircon (1.525 Å). The bulk modulus is related to both AO_8 polyhedra and BO_4 tetrahedra when their sizes are comparable, and the linear relationship stated above will not be applicable. There are obvious deviation between the observed and predicted bulk modulus for zircon (209 GPa calculated from formula (1) and more than 300 GPa for observed).[31] In scheelite-type phosphates, Sc has the smallest size (the bond distance is even smaller than Zr-O in reidite), so the compressibility should be more relied on both ScO_8 polyhedra and PO_4 tetrahedra, and the very high bulk modulus is thus understandable.

B. Raman measurements

Raman measurement of zircon and the assignment of the individual modes have been well done defined before.[34,35] Recently, a similar result on zircon-type $TbPO_4$ was reported based on polarization measurements of single crystals.[18] Group theory analysis predicts that there are 12 Raman active modes in the Brillouin zone center:

$$\Gamma = 2A_{1g} + 4B_{1g} + B_{2g} + 5E_g. \tag{2}$$

These modes can be classified as seven internal modes ($2A_{1g}+2B_{1g}+B_{2g}+2E_g$), four external translational modes ($2B_{1g}+2E_g$), and one external rotational mode (E_g). The internal modes are due to the normal vibrations of oxygen atoms within the PO_4 tetrahedra. The translational modes are generated from the translations of PO_4 tetrahedra and the larger cations (Sc^{3+}, Y^{3+}, or Ln^{3+}). The rotational mode E_g represents the rotation of whole PO_4 tetrahedral units.

Crystals of $ScPO_4$ and YPO_4 have very good Raman signals at ambient conditions, and nearly all the 12 Raman active modes can be detected. However, with the increase in pressure, the signal/noise ratio decreases dramatically, and no good signal can be detected at pressure higher than 15 GPa for the small pieces of both crystals (<10 μm). The measured Raman spectra of $ScPO_4$ and YPO_4 at various pressures are shown in Fig. 5. Above 10 GPa, the Raman signal from both samples became very weak. For $ScPO_4$, the Raman measurement could not be done at the pressure range of the transition. The Raman modes of YPO_4 above 13.4 GPa became very weak, and even the strongest A_{1g} mode (~1000 cm^{-1} at ambient conditions) could not be detected. However, a peak with a frequency a little lower than that of the A_{1g} mode appeared [marked with arrow in Fig. 5(b)], which indicated a pressure-induced phase transition in YPO_4. The smaller value of the mode from the high-pressure phase of YPO_4 is consistent with the observations of $TbPO_4$.[18] The measured phase transition of YPO_4 by Raman occurred at slightly lower pressures (14.6 GPa) than observed by XRD measurements. This is reasonable because Raman scattering

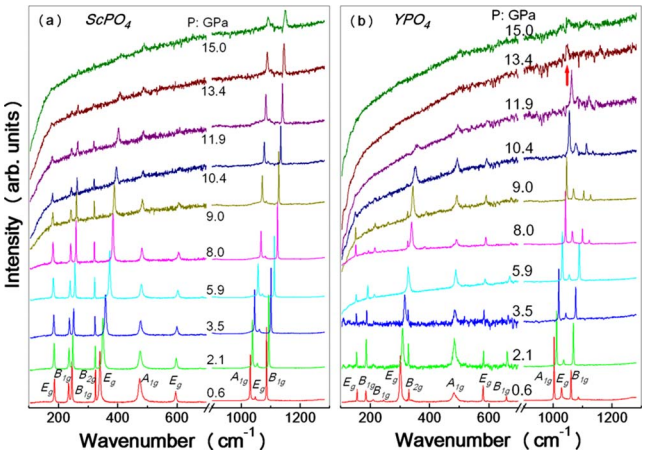

FIG. 5. (Color online) Raman spectrum of phosphates measured at different pressures (a) $ScPO_4$ and (b) YPO_4. A phase transition can be observed in YPO_4 at 13.4 GPa, and the mode marked with arrow is contributed by high-pressure phase.

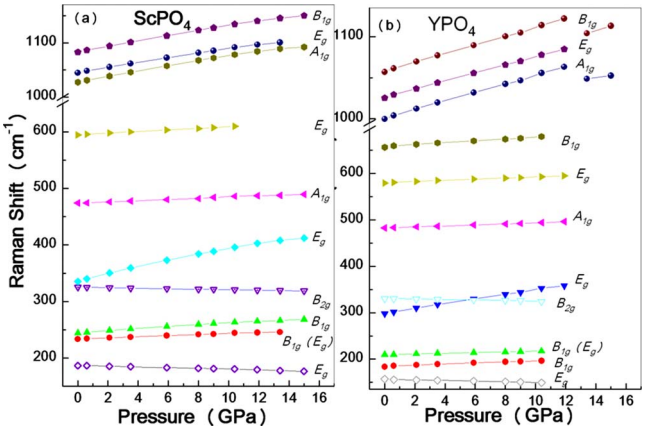

FIG. 6. (Color online) Pressure dependence of the wave number of different modes in (a) $ScPO_4$ and (b) YPO_4. The open symbols represent the soft modes.

measures the short-range order, thus, a local structural change can be detected at high pressures. The pressure dependence of the measured wave number of the vibrational modes for $ScPO_4$ and YPO_4 are shown in Fig. 6. The assignment of individual modes is based on the polarization measurements in $TbPO_4$.[18] The assignments, wave numbers of individual modes at ambient conditions, and their pressure dependence are listed in Table I. The Gruneisen parameters of the individual modes of the zircon-type phase were calculated with the formula

$$\kappa = \frac{B_0}{\omega_i}\frac{\partial \omega_i}{\partial P}, \tag{3}$$

where ω_i is the Raman wave number of the mode, and B_0 is the bulk modulus from XRD measurements. Importantly, there are two sharp modes—one external translational mode, E_g, and one internal mode, B_{2g}, which are softened at high pressures, and their wave numbers show a slight decreases with the increase in pressure. The rotational mode in the phosphate units of $ScPO_4$ and YPO_4 has the largest shift at high-pressure. This is very different from the behavior of polyhedra at elevated pressures in other solids, such as the boron-icosahedra in boron-rich solids.[36,37] In boron-rich solids, all of the B_{12} icosahedra lie along lines with the same orientation, and the compression of the structure has little effect on the rotation of the polyhedral around these lines; thus, the rotational mode is nearly pressure independent. In these phosphates, however, the PO_4 tetrahedra are separated from one another by larger cations (Sc^{3+} or Y^{3+}), and they do not lie along the same axis or have the same orientation, and thus be easily affected by external pressure.

C. Theoretical calculations

Previous experimental results revealed that the critical transition pressure and structural stability of ABO_4 com-

TABLE I. Raman active modes of $ScPO_4$ and YPO_4 at room conditions, assignments and their pressure-related Grunium parameters (κ).

		$ScPO_4$		YPO_4	
Character	Assignments	ω_0 (cm^{-1})	κ	ω_0 (cm^{-1})	K
External translational	E_g	186.7	−0.64	157.1	−0.79
	B_{1g}	233.7	0.74	183.6	1.18
	E_g (or B_{1g})	244.4	1.22	210.0	0.65
Rotational	E_g	335.4	2.86	297.9	3.16
Internal	B_{2g}	325.3	−0.25	330.1	−0.31
	A_{1g}	474.3	0.41	482.5	0.43
	E_g	594.4	0.44	579.3	0.40
	B_{1g}			656.4	0.58
	A_{1g}	1027.2	0.80	999.6	0.97
	E_g	1044.5	0.75	1025.4	0.90
	B_{1g}	1083.0	0.78	1057.0	0.94

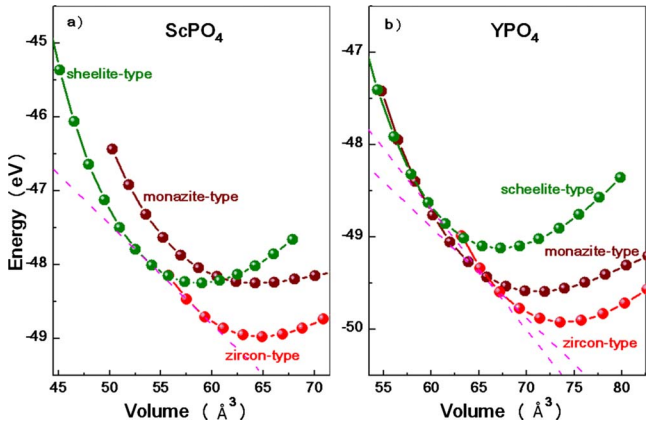

FIG. 7. (Color online) Calculated lattice energy of the different phases in (a) $ScPO_4$ and (b) YPO_4.

pounds are strongly relied on the size ratio of BO_4 tetrahedra and A cation.[16] Zircon-type structure is more stable to those compounds with larger values of size ratio. To rare-earth phosphates, only A cations with smaller size (including Sc and Y) can form zircon-type structure, and all the larger cations from La and Gd form the monazite-type structure at ambient conditions. Gadolinium phosphate is on the boundary and the critical value of the size ratio of BO_4/A is 2.65. Zircon-type phase is stable at ambient condition to those phosphates with PO_4/A size ratio larger than 2.65. Due to the small size of Sc, $ScPO_4$ has the largest size ratio (~3.3) and is thus the most stable zircon-type phosphate. In zircon-, scheelite- and monazite-type structures, rare-earth (RE) are loosely bonded with 8 or 9 neighbor anions. Under high-pressure, the RE-O bonds are easier to be compressed, compared to the strong bonded PO_4 tetrahedra. The competition and stability of the above three phases at high pressures can only be determined by quantum mechanical calculations. Our in situ XRD experiments under high-pressure for all rare-earth phosphates indicated that only Yb and Lu (also Sc) can form pure scheelite-type structures directly from the zircon-type structures at high pressures.[17] Cation Y^{3+} has similar size with Dy^{3+} and Ho^{3+}, and experiments found that zircon-type phosphates with rare-earth elements from Gd to Tm has a pressure-induced phase transition from zircon-type to monazite-type phase first and then tend to transform to the scheelite-type structure. The formation of intermediate monazite-type structure in YPO_4 at high-pressures is thus expected.

In order to further understand the different phase transition behaviors of $ScPO_4$ and YPO_4 at high-pressure, a quantum mechanical calculation was made based on density-functional theory with plane-wave basis sets using VASP. The structure of the zircon-type and the scheelite-type high-pressure phases for both samples are based on the known structural model of zircon and the XRD measurements. The initial structure of the monazite-type high-pressure phase is built on the monoclinic phase of $LaPO_4$. The calculated total energy as a function of volume of different phases of $ScPO_4$ and YPO_4 is shown in Fig. 7. The calculated bulk moduli are listed in Table II together with the measured values. The calculated values are in general agreement with our experimental observations. The calculated phase transition sequence also indicates that a monazite-type high-pressure phase of YPO_4 forms first, and the scheelite-type high-pressure phase becomes more stable at higher pressures. The calculated transition pressures from zircon-type to monazite-type YPO_4 is $P_1=15.8$ GPa, which is in good agreement with the observed value of 14.6 GPa. The calculated transition pressures to the scheelite-type, high-pressure phase in both samples (21.7 GPa for $ScPO_4$; 20.8 GPa for YPO_4) are a little less than the measured transition pressures (both greater than 30 GPa). The calculated monazite-type phase of $ScPO_4$ has a slightly smaller volume as compared with the zircon-type structure. The phase transition from zircon-type to monazite-type is difficult to induce by pressure at low temperature. The monazite-type structure of $ScPO_4$ may be a high-temperature phase. There are no reports of phases other than zircon-type structure in $ScPO_4$ and YPO_4 up to now.

IV. SUMMARY

Pressure-induced phase transitions of zircon-type $ScPO_4$ and YPO_4 were investigated by powder XRD, Raman scattering, and quantum mechanical calculations. The zircon-type phosphates transformed to scheelite-type high-pressure phases at pressures above 30 GPa in $ScPO_4$ and YPO_4. There

TABLE II. Measured and calculated bulk modulus of various structures of $ScPO_4$ and YPO_4 The measured bulk modulus is derived from the fitting of P-V curve with Birch-Murnaghan equation of state when the derivative B_0' is fixed at 4. The theoretical values are derived from the calculated energy-volume curves and pressure calibration was applied to the calculated P-V data before the bulk modulus was calculated.

	$ScPO_4$		YPO_4	
Structure	Measured	Calculated	Measured	Calculated
Zircon type	203 (7) GPa	183.0 (2.3) GPa	186 (5) GPa	165.5 (1.4) GPa
	(0–35 GPa)	$B_0'=4.2(0.2)$	(0–21 GPa)	$B_0'=4.3(0.1)$
Monazite type		188.5 (0.1) GPa	260 (29) GPa	190 (13) GPa
		$B_0'=3.3(0.1)$	(16–34 GPa)	$B_0'=2.4(3.7)$
Scheelite type	376 (8) GPa	334 (16) GPa		213.7 (1.1) GPa
	(31–50 GPa)	$B_0'=3.4(0.2)$		$B_0'=3.6(0.1)$

is a monazite-type high-pressure phase formed before the transition from zircon-type to scheelite-type structure in YPO_4 at 14.6 GPa. All the sluggish phase transitions in $ScPO_4$ and YPO_4 are displacive and reversible. The observed phase transition sequences and transition pressures for the two systems are due to the different cationic size, and consistent with the results of the quantum mechanical calculations. The very large bulk modulus of the scheelite-type high-pressure phase of $ScPO_4$ suggests that it may be a superhard material.

ACKNOWLEDGMENTS

This work was supported by the Office of Basic Energy Sciences of the U.S. Department of Energy, through Grant No. DE-FG02-97ER45656. Research at ORNL is sponsored by the Division of Materials Science and Engineering, Office of Basic Energy Sciences, US DOE, under Contract No. DE-AC05-00OR22725 with Oak Ridge National Laboratory, managed and operated by UT-Battelle, LLC. The use of the beam line at X17C and U2 station of NSLS is supported by NSF COMPRES under Contract No. EAR01-35554 and by US-DOE Contract No. DE-AC02-10886. The use of the synchrotron in the B2 station of CHESS at Cornell University is financially supported by the National Science Foundation and the National Institutes of Health/National Institute of General Medical Sciences under NSF Grant No. DMR-0225180. The synchrotron experiments performed at HPCAT (Sector 16), Advanced Photon Source (APS), Argonne National Laboratory is supported by DOE-BES, DOE-NNSA, NSF, and the W.M. Keck Foundation. APS is supported by DOE-BES under Contract No. DE-AC02-06CH11357.

*rodewing@umich.edu

[1] R. J. Finch and J. M. Hanchar, Rev. Mineral. Geochem. **53**, 1 (2003).
[2] A. F. Reid and A. E. Ringwood, Earth Planet. Sci. Lett. **6**, 205 (1969).
[3] F. X. Zhang, V. Pointeau, L. C. Shuller, D. M. Reaman, M. Lang, Z. Liu, J. Hu, W. R. Panero, U. Becker, C. Poinssot, and R. C. Ewing, Am. Mineral. **94**, 916 (2009).
[4] M. Lang, F. X. Zhang, J. Lian, C. Trautmann, R. Neumann, and R. C. Ewing, Earth Planet. Sci. Lett. **269**, 291 (2008).
[5] S. V. Ushakov, K. B. Helean, A. Navrotsky, and L. A. Boatner, J. Mater. Res. **16**, 2623 (2001).
[6] J. B. Davis, D. B. Marshall, R. M. Housley, and P. E. D. Morgan, J. Am. Ceram. Soc. **81**, 2169 (1998).
[7] J. B. Davis, D. B. Marshall, and P. E. D. Morgan, J. Eur. Ceram. Soc. **20**, 583 (2000).
[8] R. C. Ewing and L. Wang, Rev. Mineral. Geochem. **48**, 673 (2002).
[9] L. A. Boatner, G. W. Beall, M. M. Abraham, C. B. Finch, P. G. Huray, and M. Rappaz, Bull. Am. Phys. Soc. **25**, 186 (1980).
[10] J. G. Pepin, E. R. Vance, and G. J. McCarthy, Mater. Res. Bull. **16**, 627 (1981).
[11] A. J. Wojtowicz, D. Wiskiewski, A. Lempicki, and L. A. Boatner, Radiat. Eff. Defects Solids **135**, 305 (1995).
[12] A. Lempicki, E. Berman, A. J. Wojtowicz, M. Balcerzyk, and L. A. Boatner, IEEE Trans. Nucl. Sci. **40**, 384 (1993).
[13] W. W. Moses, M. J. Weber, S. E. Derenzo, D. Perry, P. Berdahl, and L. A. Boatner, IEEE Trans. Nucl. Sci. **45**, 462 (1998).
[14] F. Dachille and L. S. D. Glasser, Acta Crystallogr. **12**, 820 (1959).
[15] O. Fukunaga and S. Yamaoka, Phys. Chem. Miner. **5**, 167 (1979).
[16] D. Errandonea and F. J. Manjon, Prog. Mater. Sci. **53**, 711 (2008).
[17] F. X. Zhang, M. Lang, R. C. Ewing, J. Lian, Z. W. Wang, J. Hu, and L. A. Boatner, J. Solid State Chem. **181**, 2633 (2008).
[18] A. T. E. Stavrou, Y. C. Boulmetis, A. G. Kontos, Y. S. Raptis, and C. Raptis, J. Phys.: Condens. Matter **20**, 395222 (2008).
[19] A. P. Hammersley, FIT2D, ESRF, Grenoble, France, 1998.
[20] H.-K. Mao, J. Xu, and P. M. Bell, J. Geophys. Res. **91**, 4673 (1986).
[21] J. Rodriguez-Carvajal, Fullprof 2k, France, 2001.
[22] J. Hafner, Comput. Phys. Commun. **177**, 6 (2007).
[23] P. E. Blöchl, Phys. Rev. B **50**, 17953 (1994).
[24] J. P. Perdew, J. A. Chevary, S. H. Vosko, K. A. Jackson, M. R. Pederson, D. J. Singh, and C. Fiolhais, Phys. Rev. B **46**, 6671 (1992).
[25] J. P. Perdew and Y. Wang, Phys. Rev. B **45**, 13244 (1992).
[26] J. P. Perdew and Y. Wang, Phys. Rev. B **33**, 8800 (1986).
[27] W. van Westrenen, M. R. Frank, J. M. Hanchar, Y. Fei, R. J. Finch, and C.-S. Zha, Am. Mineral. **89**, 197 (2004).
[28] E. Knittle and Q. Williams, Am. Mineral. **78**, 245 (1993).
[29] A. Grzechnik, K. Syassen, I. Loa, M. Hanfland, and J. Y. Gesland, Phys. Rev. B **65**, 104102 (2002).
[30] S. Ono, K. Funakoshi, Y. Nakajima, Y. Tange, and T. Katsura, Contrib. Mineral. Petrol. **147**, 505 (2004).
[31] H. P. Scott, Q. Williams, and E. Knittle, Phys. Rev. Lett. **88**, 015506 (2001).
[32] R. M. Hazen and C. T. Prewitt, Am. Mineral. **62**, 309 (1997).
[33] D. Errandonea, J. Pellicer-Porres, F. J. Manjón, A. Segura, Ch. Ferrer-Roca, R. S. Kumar, O. Tschauner, P. Rodríguez-Hernández, J. López-Solano, S. Radescu, A. Mujica, A. Muñoz, and G. Aquilanti, Phys. Rev. B **72**, 174106 (2005).
[34] P. Dawson, M. M. Hargreave, and G. R. Wilkinson, J. Phys. C **4**, 240 (1971).
[35] A. Gucsik, M. Zhang, C. Koeberl, E. K. H. Salje, S. A. T. Redfern, and J. M. Pruneda, Mineral. Mag. **68**, 801 (2004).
[36] D. R. Tallant, T. L. Aselage, A. N. Campbell, and D. Emin, Phys. Rev. B **40**, 5649 (1989).
[37] F. X. Zhang, Chem. Phys. Lett. **379**, 47 (2003).